Available online at www.sciencedirect.com

ScienceDirect

Geochimica et Cosmochimica Acta 140 (2014) 509–520

Geochimica et Cosmochimica Acta

www.elsevier.com/locate/gca

First-principles calculations of equilibrium silicon isotope fractionation among mantle minerals

F. Huang [a,*], Zhongqing Wu [b,c,*], Shichun Huang [d], Fei Wu [a]

[a] CAS Key Laboratory of Crust-Mantle Materials and Environments, School of Earth and Space Sciences, University of Science and Technology of China, Hefei, Anhui 230026, China

[b] Laboratory of Seismology and Physics of Earth's Interior, School of Earth and Space Sciences, University of Science and Technology of China, Hefei, Anhui 230026, China

[c] Mengcheng National Geophysical Observatory, Anhui, China

[d] Department of Geoscience, University of Nevada Las Vegas, 4505 S. Maryland Parkway, Las Vegas, NV 89154-4010, United States

Received 26 January 2014; accepted in revised form 22 May 2014; available online 5 June 2014

Abstract

Silicon isotope fractionation factors for mantle silicate minerals, including olivine, wadsleyite, ringwoodite, pyroxenes, garnet (pyrope), majorite, and Mg-perovskite, are calculated using density functional theory. Our results show that equilibrium fractionations of Si isotopes are negligible among pyroxenes, olivine, and pyrope, but are significant between olivine and its polymorphs (wadsleyite and ringwoodite). There is also significant Si isotope fractionations between mantle minerals with different Si coordination numbers (CN), such as Mg-perovskite (CN = 6) and olivine polymorphs (CN = 4). When in equilibrium with each other, $^{30}Si/^{28}Si$ decreases in the order of olivine > pyroxenes > wadsleyite > majorite > ringwoodite > Mg-perovskite.

Our calculation predicts significant Si isotope fractionation between mantle minerals, e.g., perovskite vs. ringwoodite, majorite vs. pyroxene, and olivine vs. its polymorphs even at high pressure and temperature conditions of deep mantle. The Si CN in silicate melt increases with increasing pressure, implying that Si isotope fractionation between silicate and metal could be a function of pressure. Our results suggest that Si isotopic fractionation factor between silicate and metal may decrease with increasing pressure; consequently, Si isotopic fractionation factor obtained from low pressure experiments may not be applicable to Si isotope fraction during core formation which occurred at high pressure. Finally, Si isotopes could also be fractionated between perovskite-rich mantle and residual melt during magma-ocean cooling in the lower mantle because of their different Si CNs. If such primordial signature is not destroyed and partially preserved through the Earth's history, significant Si isotope heterogeneity could still exist between the upper and lower mantle.

1. INTRODUCTION

Silicon is the second most abundant element of the Earth as a major element in the crust and mantle, and likely an important light element in the core (Mcdonough and Sun, 1995; McDonough, 2003). Recent advances in high precision analyses using MC-ICP-MS have revealed significant Si isotopic variations in both terrestrial and extra-terrestrial samples (Georg et al., 2007; Fitoussi et al., 2009; Armytage et al., 2011, 2012; Zambardi and Poitrasson, 2011; Fitoussi and Bourdon, 2012; Pringle et al., 2013; Savage et al., 2010, 2011, 2012, 2013a, 2014; Zambardi et al., 2013). Although Earth and enstatite

* Corresponding authors. Tel.: +86 551 63607810 (F. Huang), +86 551 63607975 (Z.-Q. Wu).

E-mail addresses: fhuang@ustc.edu.cn (F. Huang), wuzq10@ustc.edu.cn (Z. Wu).

http://dx.doi.org/10.1016/j.gca.2014.05.035

0016-7037/

chondrites have the same isotopic compositions for many elements (see a summary in Javoy et al., 2010; Kaminski and Javoy, 2013), the possible Si isotopic difference between terrestrial rocks and enstatite chondrites is attributed to a number of fundamental processes including the accretion of the Earth, core–mantle differentiation, and Moon formation (e.g., Georg et al., 2007; Fitoussi et al., 2009; Savage et al., 2010; Armytage et al., 2011, 2012; Pringle et al., 2013; Savage and Moynier, 2013; Zambardi et al., 2013). Furthermore, Si isotopes have also been used to study high temperature geochemical processes to constrain continent formation and mantle evolution (Armytage et al., 2011, 2012; Savage et al., 2010, 2011, 2012, 2013a).

Theoretical calculation and analytical work clearly demonstrate that stable isotopes of many elements, such as O, Mg, Fe, and Ca, can be substantially fractionated among silicate minerals according to their different crystalline structures at the mantle's temperature and pressure conditions (e.g., Méheut et al., 2007, 2009; Polyakov, 2009; Rustad and Yin, 2009; Huang et al., 2010, 2013; Schauble, 2011; Méheut and Schauble, 2014). We are interested in whether Si joins into this group of elements that show substantial isotopic fractionation among silicate minerals. This has fundamental implications in understanding Si isotope composition of the bulk silicate Earth (BSE).

In addition, several recent high pressure experiments (up to 7 GPa) found significant Si isotope fractionations between silicates and metallic melt, up to 0.5‰ per amu difference at 2200 °C and 7 GPa (e.g., Shahar et al., 2009, 2011; Ziegler et al., 2010; Kempl et al., 2013; Hin et al., 2014). However, such data may not be directly applied to Si isotope fractionation during core formation because core–mantle segregation occurred at much higher pressure (above 25 GPa) (Li and Agee, 1996; Wade and Wood, 2005). That is, is Si isotopic fractionation between silicate and metal sensitive to pressure?

To answer these questions, we systematically investigated Si isotope fractionations among silicate minerals over a large pressure–temperature region (up to 100 GPa and 3000 K for Mg-perovskite and 25GPa and 3000 K for other minerals). In detail, we use first-principles calculations based on density functional theory to estimate equilibrium Si isotope fractionations among major mantle silicate minerals, including olivine and its polymorphs, pyroxenes, and garnets (where Si is fourfold coordinated in the upper mantle) and Mg-perovskite with sixfold coordinated Si in the lower mantle (Table 1; Fig. 1). We also calculated fractionation factors for majorite where three-fourths of Si atoms are fourfold coordinated and one-fourth is sixfold coordinated. This study for the first time provides systematic calculations of Si isotope fractionation factors for silicate minerals at the pressure–temperature conditions of transition zone and the lower mantle, and reveals significant Si isotope fractionations among mantle minerals due to their different mineral structures and Si–O bond strength. With such data, we will discuss whether the mantle is isotopically heterogeneous and to what extent Si isotopes are fractionated among minerals with increasing pressure in the deep mantle.

2. METHODS

The equilibrium fractionation of Si isotopes can be obtained by calculating the changes in vibrational (phonon) frequencies of Si–O bonds due to isotopic substitution (Bigeleisen and Mayer, 1947; Urey, 1947; Kieffer, 1982). The reduced partition function ratio β of Si isotopes ($10^3 \ln \beta$, where β is the equilibrium fractionation factor of $^{30}Si/^{28}Si$ between a mineral and atomic Si vapor) can be calculated from:

Table 1
Polynomial fits to the reduced partition function ratios for $^{30}Si/^{28}Si$ ($10^3 \ln \beta_{30-28}$) in mantle minerals at 0, 10, and 20 GPa.

	Formula	Si–O bond length (Å)	Pressure (GPa)	A	B	C
Olivine	$^{VI}Mg_2{}^{IV}SiO_4$	1.643	0	−0.952	1.417	6.749
			10	−0.607	0.840	7.491
Wadsleyite	$^{VI}Mg_2{}^{IV}SiO_4$	1.660	0	−0.937	1.471	5.966
			10	−0.768	1.162	6.653
Clinopyroxene	$^{VIII}Ca{}^{VI}Mg{}^{IV}Si_2O_6$	1.642	0	−0.645	0.940	6.795
			10	−0.524	0.700	7.447
Orthopyroxene	$^{VI}Mg{}^{IV}SiO_3$	1.641	0	−0.455	0.647	6.985
			10	−0.520	0.697	7.513
Pyrope	$^{VIII}Mg_3{}^{VI}Al_2{}^{IV}Si_3O_{12}$	1.640	0	−0.468	0.711	6.912
			10	−0.681	1.035	7.278
Ringwoodite	$^{VI}Mg_2{}^{IV}SiO_4$	1.669	0	−0.890	1.430	5.575
			10	−0.794	1.240	6.226
			20	−0.725	1.094	6.809
Majorite	$^{VIII}Mg_3{}^{VI}[MgSi]^{IV}Si_3O_{12}$	1.677	0	−0.677	1.076	6.013
			10	−0.723	1.114	6.573
			20	−0.716	1.061	7.124
Mg-perovskite	$^{VIII}Mg{}^{VI}SiO_3$	1.800	0	−1.264	2.131	3.462
			10	−1.114	1.864	4.119
			20	−1.008	1.671	4.701

The polynomial fit uses equation form: $10^3 \ln(\beta_{30-28}) = Ax^3 + Bx^2 + Cx$ ($x = 10^6/T^2$, T is temperature in Kelvin) based on calculated reduced partition function ratios from 1000 K to 3020 K. The calculation averaged over all crystallographic Si-sites. Si–O bond lengths are average of all crystallographic Si-sites calculated at 0 GPa and 300 K, which are well consistent with literature values (Anderson, 1989).

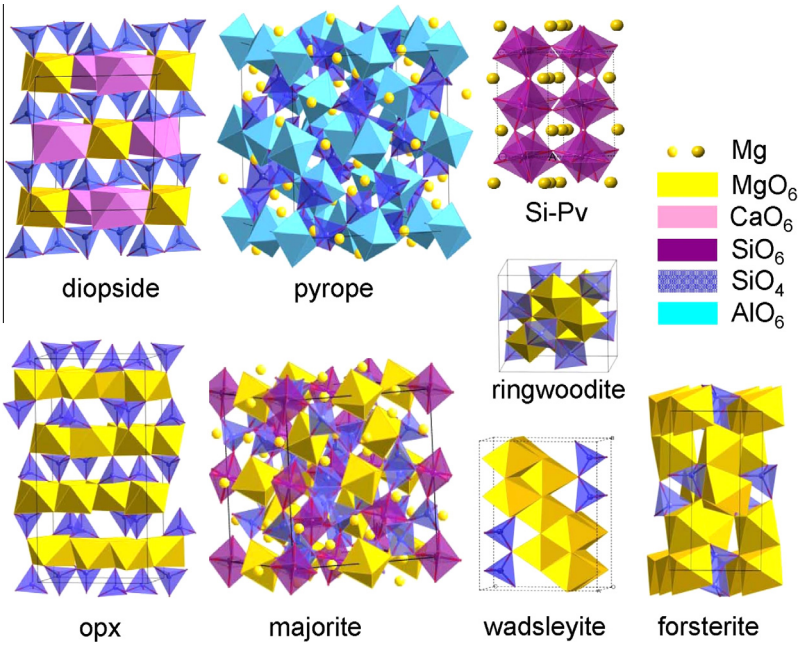

Fig. 1. The mineral structures of olivine ($Mg_2^{IV}SiO_4$), wadsleyite ($Mg_2^{IV}SiO_4$), ringwoodite ($Mg_2^{IV}SiO_4$), orthopyroxene ($Mg^{IV}SiO_3$), clinopyroxene ($CaMg^{IV}Si_2O_6$), pyrope ($Mg_3Al_2^{IV}Si_3O_{12}$), majorite ($Mg_3^{VI}[MgSi]^{IV}Si_3O_{12}$), and perovskite ($Mg^{VI}SiO_3$).

$$\beta_A = \left(\frac{Q^*}{Q}\right) = \prod_i^{3N-3} \frac{u_i^*}{u_i} \frac{e^{-\frac{1}{2}u_i^*}}{\left(1-e_i^{-u_i^*}\right)} \frac{(1-e^{-u_i})}{e^{-\frac{1}{2}u_i}} \quad (1)$$

In this equation, Q is the vibrational partition function, asterisk refers to the heavy isotope, $\mu_i = hv_i/k_BT$, where v_i is vibrational (phonon) frequency of mode i, k_B is Boltzmann constant, and T is the temperature in Kelvin. The equilibrium constant for isotopic exchange between materials A and B is given as:

$$1000 \ln \alpha_{A-B} = 1000(\ln \beta_A - \ln \beta_B). \quad (2)$$

The calculation details used here follow that used by Huang et al. (2013). We used Quantum espresso software package to calculate electric structures and phonon frequencies of materials (Giannozzi et al., 2009; Wentzcovitch et al., 2010). Local density approximation (LDA) for exchange correlation functional was used (Perdew and Zunger, 1981). The pseudo-potential for Al and Ca were generated following (Vanderbilt, 1990) with a valence configuration of $3s^23p^1$ and a cutoff radii of 1.77 bohr for Al and $3s^23p^64s^1$ and 1.85 bohr for Ca. The Mg pseudo-potential was generated using the method of von Barth and Car (Dal Corso et al., 1993) with a cutoff radii of 2.5 bohr for all channels and five configurations, $3s^23p^0$, $3s^13p^1$, $3s^13p^{0.5}3d^{0.5}$, $3s^13p^{0.5}$, and $3s^13d^1$ with decreasing weights of 1.5, 0.6, 0.3, 0.3, and 0.2, respectively. The O and Si pseudopotentials were generated following Troullier and Martins (1991), with a valence configuration of $2s^22p^4$ and a cutoff radii of 1.45 bohr for O and $3s^23p^43d^0$ and 1.47 bohr for Si. The plane-wave cutoff energy is 70 Ry. Brillouin zone summations over electronic states were calculated using $N_1 \times N_2 \times N_3$ k mesh with N_i varying with minerals (Table S1).

The initial crystal structures were obtained from American Mineralogist Crystal Structure Database (http://rruff.geo.arizona.edu/AMS/amcsd.php). Their structures under various pressures (or volumes) were well optimized using variable cell shape molecular dynamics (Wentzcovitch, 1991). Dynamical matrices were computed on a regular q mesh using density-functional perturbation theory (DFPT) (Baroni et al., 2001) and then interpolated into a dense q mesh to obtain the vibrational density of state of minerals. The sizes of the regular and dense q mesh also depend on materials (Table S1). The vibrational and thermodynamic properties for some minerals reported in previous studies were based on similar phonon calculations (Tsuchiya et al., 2004; Yu and Wentzcovitch, 2006; Li et al., 2007; Wu and Wentzcovitch, 2007; Wu et al., 2008; Yu et al., 2008, 2010, 2011). The calculated phonon frequencies agree well with the experimental measurement (e.g., see Huang et al., 2013; Table S4). The frequency scaling factors are very close to 1 (0.9967) based on the calculated phonon frequencies for pyrope, diopside, majorite, forsterite, and orthoenstatite. Furthermore, Li et al. (2009) pointed out that experimental frequency is not harmonic frequency and thus scaling treatment based on experimental frequencies is inappropriate. Therefore, we did not adopt the scaling treatment on the calculated phonon frequencies.

We used pressure as a control parameter to optimize the crystal structure under certain pressure. This is a static pressure for the optimized structure. When considering the temperature effect on pressure, expressing β as a function of pressure and temperature requires the equation of state (EOS), $P(V, T)$, which can be derived from Helmholtz free energy given by:

$$F(V,T) = U(V) + \sum_{qj} \frac{\hbar\omega_{qj}(V)}{2} + K_B T \sum_{qj} \ln\left(1 - \exp\left[\frac{\hbar\omega_{qj}(V)}{K_B T}\right]\right), \quad (3)$$

where q is a wave vector in the first Brillouin zone, j is an index of phonon mode with frequency ω_{qj}, V and T are the volume and temperature of the system, and K_B and $\hbar$ are the Boltzmann and Planck constants, respectively. The first, second, and third terms in Eq. (3) are the static internal, zero-point, and vibrational energy contributions, respectively. The calculated Helmholtz free energy versus volume is fitted by the third-order Birch–Murnaghan finite strain equation of states.

3. RESULTS

The calculated crystal structure parameters for the volume at 0GPa and 300 K, including Si–O bond lengths, for mantle silicate minerals, presented in Tables 2 and 3, are consistent with experimental data (Anderson, 1989). For example, our calculated average Si–O bond lengths of forsterite, wadsleyite, and ringwoodite agree with experimental values within ±0.5% (Table 3), with all the calculated Si–O bond lengths being systematically, but marginally, larger than the experimentally determined bond lengths for all three phases. Our calculation also reproduces the bond variation estimated using structure transformation (Tables 2 and 3).

Table 3
Comparisons of Si–O average bond lengths of forsterite, wadsleyite, and ringwoodite at ambient condition with literature data.

	Calculated (Å)	Experimental (Å)
Forsterite	1.6427	1.6346[a], 1.6362[b]
Wadsleyite	1.6596	1.6507[c],1.654[d]
Ringwoodite	1.6692	1.6649[e]

Data source: a, Hazen (1976); b, Hushur et al. (2009); c, Horiuchi and Sawamoto (1981); d, Hazen et al. (2000); and e, Hazen et al. (1993). Our results are consistent with experimental data within error (e.g., ~0.006 Å in Hazen et al. (2000)).

Table 2
The crystal lattice parameters based on quasi-harmonic approximation for the volume at 0 GPa and 300 K compared with experimental measurements.

	a (Å)	b (Å)	c (Å)	β (°)	V (Å^3)	
Diopside	9.713	8.857	5.225	105.414	437.37	Huang et al. (2013)
	9.745	8.899	5.251	105.63	438.532	Experiment[a]
	−0.3	−0.5	−0.5	−0.2	−0.3	Error (%)
Majorite $I4_1/a$	11.5284	11.5284	11.4207		1517.86	Huang et al. (2013)
	11.501	11.501	11.48		1518.6	Experiment[b]
	0.2	0.2	−0.5		0.05	Error (%)
Pyrope	11.4276				1492.322	Huang et al. (2013)
	11.459				1504.67	Experiment[c]
	−0.3				−0.8	Error (%)
Orthenstatite Pbca	18.2154	8.8305	5.1736		832.179	Huang et al. (2013)
	18.251	8.814	5.181		833.438	Experiment[d]
	−0.2	0.2	−0.2		−0.2	Error (%)
Forsterite Pnma	4.759	10.200	5.982		290.403	Huang et al. (2013)
	4.752	10.192	5.978		289.529	Experiment[e]
	0.2	0.1	0.1		0.3	Error (%)
Wadsleyite $I4_1/a$	5.7154	11.4591	8.2657		541.35	This study
	5.6978	11.4620	8.2572		539.26	Experiment[f]
	0.3	−0.02	0.1		0.4	Error (%)
Ringwoodite	8.079				527.4	This study
	8.076				526.7	Experiment[g]
	0.04				0.1	Error (%)
Periclase	4.219				75.1	This study
	4.212				74.71	Experiment[h]
	0.2				0.5	Error (%)
Mg-perovskite	4.7948	4.9458	6.9207		164.1	This study
	4.7782	4.9295	6.8984		162.5	Experiment[i]
	0.3	0.3	0.3		1	Error (%)

Data source for experimental work: a, Cameron et al. (1973); b, Angel et al. (1989); c, Gibbs and Smith (1965); d, Yang and Ghose (1995); and e, Kirfel et al. (2005).f, Hazen et al. (2000); g, Meng et al. (1994); h, Dewaele et al. (2000); i, Mao et al. (1991).

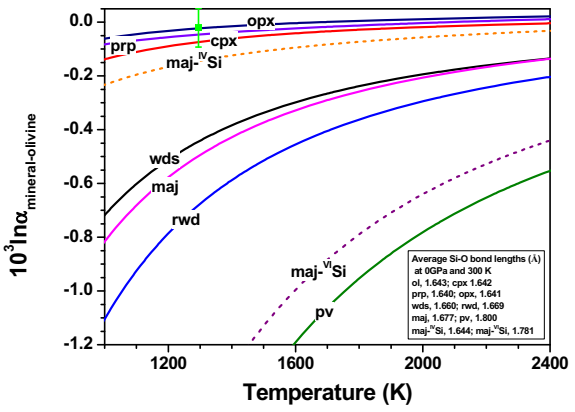

Fig. 2. Variations of equilibrium fractionation coefficients ($10^3\ln\alpha_{mineral–olivine}$) with temperature at 0 GPa. Relative enrichment order of heavy isotopes is consistent with decreasing the average Si–O atomic bond lengths calculated at 300 K and 0 GPa (see Table 1). Mineral abbreviations: opx, orthopyroxene; cpx, clinopyroxene; ol, olivine; maj, majorite; prp, pyrope; wds, wadsleyite; rwd, ringwoodite; and pv, Mg-perovskite. Maj-^{IV}Si and maj-^{VI}Si stand for the Si atom in majorite with CN of 4 and 6, respectively. Because the length of ^{VI}Si–O in majorite is much longer than that of ^{IV}Si–O, the average of four Si–O bonds of majorite is longer than that of ringwoodite. The maj-^{IV}Si curve is the average of the three ^{IV}Si–O bonds in majorite (Table 2). Note that $10^3\ln\alpha_{mineral–olivine}$ is equivalent to $\Delta^{30}Si_{mineral–olivine}$.

Table 1 summarizes the reduced partition function ratios of silicon isotopes ($10^3\ln\beta$) of mantle minerals at 0, 10, and 20 GPa as a function of temperature. $10^3\ln\beta$ and Si isotope fractionation factor between two phases A and B ($10^3\ln\alpha_{A–B}$) decrease dramatically with increasing temperature (Fig. 2). The fractionation factor between Phases A and B is defined as $10^3\ln\alpha_{A–B} = 10^3\ln(\beta_A/\beta_B) = \delta^{30}Si_A - \delta^{30}Si_B = \Delta^{30}Si_{A–B}$, and $\delta^{30}Si_A = [(^{30}Si/^{28}Si)_A/(^{30}Si/^{28}Si)_{standard} - 1] * 1000$ (‰). Our results show that wadsleyite, majorite, ringwoodite, and perovskite have much lighter Si isotope compositions compared to olivine, pyrope, and pyroxenes when they are in equilibrium with each other. Heavy Si isotopes are enriched in the order of

olivine > orthopyroxene > pyrope > clinopyroxene

although fractionations among these minerals are small (<0.1‰) at temperature above 1000 °C. The negative $\Delta^{30}Si_{clinopyroxene–olivine}$ predicted in our calculations (Fig. 2) is consistent with recent observations in peridotite xenoliths and layered mafic intrusions (Georg et al., 2007; Savage et al., 2011). The negative $\Delta^{30}Si_{orthopyroxene–olivine}$ is consistent with the results in Méheut et al. (2009) and Méheut and Schauble (2014). Nevertheless, the magnitudes of Si isotope fractionation between orthopyroxene and olivine in both studies are very small at high temperature (<0.05‰ at 1000 °C).

4. DISCUSSION

4.1. Controlling Si isotope fractionation by crystal structure

A shorter bond is generally stronger with higher vibrational energy, and thus when equilibrium, it is more enriched in heavy isotopes than a longer bond (Urey, 1947). The Si–O bond lengths increase in the order of olivine < wadsleyite < ringwoodite (Table 1), consistent with the order of ^{30}Si depletion from olivine to wadsleyite and then to ringwoodite (Fig. 2). Our calculation shows that Si isotopes can be fractionated between minerals with identical Si CN if their bonding strength and Si–O bond lengths are different.

The largest Si isotope fractionation occurs between minerals with different CN of Si. When in equilibrium, perovskite, with a Si CN of six, has significantly lighter Si isotopic composition than minerals with a Si CN of four (such as pyroxenes, olivine-polymorphs, garnet, and majorite) (Fig. 2). Our calculation shows $\Delta^{30}Si_{olivine\text{-}perovskite} = 1.2‰$ at zero pressure and 1600 K, which can be well resolved with the current analytical precision (~0.05‰amu^{-1}) (Fitoussi et al., 2009; Savage et al., 2010, 2011; Zambardi and Poitrasson, 2011). In majorite, ^{VI}Si, Si in an octahedral site with a CN of six, is also isotopically lighter than ^{IV}Si, Si in a tetrahedral site with a CN of four, further confirming large Si isotope fractionation between Si with different CNs (Fig. 2). Because Si^{4+} is not adjacent to Al^{3+} which substitutes ^{VI}Si in the majorite structure (i.e., ^{IV}Si–O tetrahedron in majorite structure in Fig. 1), the presence of Al^{3+} may not significantly modify fractionation factors of Si isotopes. For example, the replacement of a ^{VI}Si atom and a ^{VI}Mg atom by 2 Al atoms during the transformation of majorite to pyrope only slightly increases $\Delta^{30}Si_{mineral–olivine}$ for ^{IV}Si from −0.095 to −0.023 at 1600 K (Fig. 2). In detail, $\Delta^{30}Si_{prp\text{-}maj}$ ^{IV}Si is only ~one tenth of $\Delta^{30}Si_{maj}$ $^{IV}Si_{\text{-}maj}$ ^{VI}Si.

At present day geotherm, orthopyroxene ($^{VI}Mg^{IV}SiO_3$) and clinopyroxene ($^{VIII}Ca^{VI}Mg^{IV}Si_2O_6$) gradually transform into a garnet-like phase with increasing pressure until pyroxenes disappear at ~480 km depth in the Earth's mantle (Agee, 1993), while majorite ($^{VIII}Mg_3{}^{VI}[MgSi]^{IV}Si_3O_{12}$) continuously reacts with pyrope to form a majorite garnet solid solution (Anderson, 1989; Agee, 1993). Our calculations show that the three fourfold coordinated Si atoms in majorite have $10^3\ln\beta$ similar to olivine and pyroxenes, but much higher than the Si with a CN of six (Fig. 1, Table 4). If they are in equilibrium with each other, taking into account of all four Si atoms, majorite is isotopically lighter than pyroxenes, olivine, and pyrope (Table 1 and Fig. 2). Because of the same reason, the lower Si CN in ringwoodite compared to perovskite (IV vs. VI) implies

Table 4
Polynomial fits to the reduced partition function ratios for $^{30}Si/^{28}Si$ ($10^3\ln\beta$) for majorite at 0 GPa and from 1000 K to 3020 K. ^{VI}Si and ^{IV}Si in majorite ($^{VIII}Mg_3{}^{VI}[MgSi]^{IV}Si_3O_{12}$) are also listed for a comparison.

Mineral	Si–O length (Å)	A	B	C
Majorite	^{VI}Si, 1.781	−0.7743	1.3162	4.2215
	^{IV}Si-1, 1.641	−0.6004	0.9069	6.8654
	^{IV}Si-2, 1.639	−0.8833	1.4003	6.3686
	^{IV}Si-3, 1.646	−0.5950	0.9173	6.6074

The polynomial fit uses the equation form: $10^3\ln(\beta_{30–28}) = Ax^3 + Bx^2 + Cx$, where $x = 10^6/T^2$. T is temperature in Kelvin. ^{VI}Si stands for the sixfold coordinated Si atom in majorite, while ^{IV}Si-1, ^{IV}Si-2, and ^{IV}Si-3 are the three fourfold coordinated Si atoms.

significant enrichment of heavy Si isotopes in ringwoodite relative to perovskite (Fig. 2, Table 3).

4.2. Effects of pressure and temperature on Si isotope fractionation

Varying pressure may cause changes in mineral structures, as well as bonding environment, which in turn affects isotope fractionation factors (Horita et al., 2002; Clayton, 2007; Polyakov, 2009; Huang et al., 2013). In order to better constrain stable isotope variations in the deep mantle, it is necessary to address the pressure effect on equilibrium isotope fractionation between minerals and melts. Our results revealed the pressure effect on equilibrium isotope fractionation because the Si–O bonding strengths and vibrational frequencies are related to pressure (Table 1). If the vibrational frequency difference between two minerals decreases with increasing pressure, the inter-mineral isotope fractionation also decreases. This is the case for inter-mineral fractionations between olivine and wadsleyite, and between ringwoodite and Mg perovskite (Fig. 3). Unlike fractionation of Mg isotopes which is sensitive to pressure (Huang et al., 2013), there is a much smaller pressure effect on Si isotope fractionation between silicate minerals. This

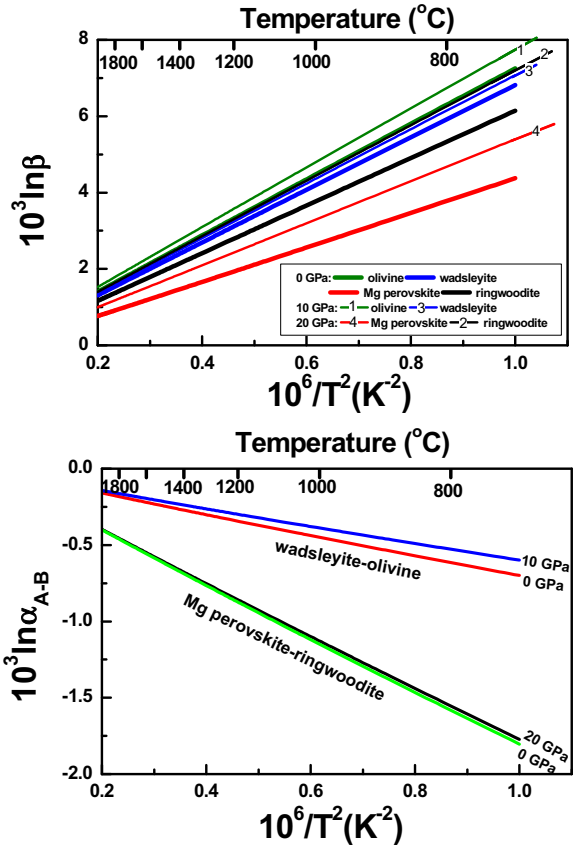

Fig. 3. The pressure effect on (a) reduced partition function ratios of wadsleyite, olivine, ringwoodite, and Mg-perovskite (pv) and (b) equilibrium fractionation factors ($10^3 \ln \alpha_{\text{wadsleyite–olivine}}$ and $10^3 \ln \alpha_{\text{ringwoodite–pv}}$). Because the pressure effect on bonding strengths varies in different minerals, pressure can modify inter-mineral isotope fractionation. Data are from Table 1.

may reflect different bonding environments of Si and Mg cations in minerals: Si is at the center of Si–O tetrahedrons (e.g., in olivine) or octahedrons (e.g., in perovskite), while Mg is combined with non-bridge oxygen at the edge of Si–O tetra-octahedrons.

Recent experiments at 1 and 7 GPa revealed negligible Si isotope fractionation between silicate melt and olivine (Shahar et al., 2011). In this pressure range, Si in silicate melt is dominantly fourfold coordinated (Stixrude and Karki, 2005). Therefore, it is possible that Si isotope fractionation between silicate melt and minerals with the same Si CN is negligible. At higher pressure, theoretical calculations and experimental study revealed that Si CN in melt increases from 4 to 6 when pressure increases from zero to 50 or 125 GPa (Stixrude and Karki, 2005; Sanloup et al., 2013). Therefore, increasing pressure may have large effect on $\Delta^{30}Si_{\text{mineral-melt}}$ because of the significant pressure effect on Si CNs in the melt (Stixrude and Karki, 2005; Sanloup et al., 2013).

Our results can be used to estimate the pressure effect on Si isotope fractionation between silicate and metallic melt. Georg et al. (2007) argued that Si isotope fractionation factors between silicate and metal calculated at $\sim 10^5$ Pa may be larger than that at higher pressure, where the dominant Si-bearing phase is perovskite with a Si CN of 6. Hence, the silicate–metal isotope fractionation factor calculated at 10^5 Pa may not be applicable in constraining the Si isotope fractionation during core–mantle segregation which occurred at much higher pressure (Wade and Wood, 2005). Our calculation clearly shows that olivine is enriched in heavy Si isotopes than wadsleyite and ringwoodite, which are further heavier than perovskite (Fig. 2). It is not clear yet how pressure affects Si coordination state and isotope fractionation factor in metallic melt. Since no phase transition of iron crystal occurs at the pressure–temperature conditions around mantle transition zone (Boehler, 2000), it is likely that pressure has a negligible effect on the isotope fractionation factor of metallic melt at the pressure intervals where core–mantle segregation occurred. If the core formed at the pressure and temperature regions where the Si CN in silicate melt is great than 4 (e.g., at ~3750 K and 40 GPa in Wade and Wood (2005)), then Si isotope fractionation factors ($\Delta^{30}Si_{\text{silicate–metal}}$) at high pressure may be smaller than those determined at low pressure (e.g., 10_5 Pa). Therefore, $\Delta^{30}Si_{\text{silicate–metal}}$ measured at low pressures (e.g., Shahar et al., 2011; Hin et al., 2014) may not be applied to constrain Si content of the core.

4.3. Si isotope fractionation in the mantle

The relationships between stable isotopic compositions of the Earth and that of the primitive and differentiated meteorites have provided a plethora of important information about the bulk composition and evolution history of the Earth (e.g., Clayton, 2007; Georg et al., 2007; Chakrabarti and Jacobsen, 2010; Savage et al., 2010; Armytage et al., 2011; Moynier et al., 2011; Fitoussi and Bourdon, 2012). Although no significant Si isotopic variation is reported in the upper mantle materials (Fitoussi et al., 2009; Savage et al., 2010, 2013b), our calculation

suggests possible per mil level Si isotope heterogeneity among mantle minerals. Since garnets (pyrope and majorite) coexist with olivine and pyroxenes in a broad pressure and temperature range (Kaminsky, 2012), Si isotopic fractionations between garnets and olivine/pyroxenes vary with depth (Fig. 4).

The magnitude of isotope fractionation between mantle minerals depends on the geothermal gradient. Along the present day geothermal gradient, Si isotope fractionations among pyroxenes, olivine, and pyrope are less than 0.1‰, well consistent with observations in minerals from mantle peridotites s (~0.1‰, 2σ) (Georg et al., 2007; Chakrabarti and Jacobsen, 2010), while substantial fractionation can occur during olivine polymorphic transitions with $\Delta^{30}Si_{olivine-wadsleyite} = 0.24‰$ at 410 km (1730 K) and $\Delta^{30}Si_{wadsleyite-ringwoodite} = 0.12‰$ at 520 km (1814 K, see Table 5 for details of present day geothermal gradient). Most importantly, Mg-perovskite is significantly lighter than ringwoodite and majorite with $\Delta^{30}Si_{ringwoodite-perovskite} = 0.54‰$ and $\Delta_{30}Si_{majorite-perovskite} = 0.63‰$ at 670 km (~24 GPa and 1900 K) at the present day geothermal gradient (Table 5), implying large fractionation following the reaction of Mg_2SiO_4 (ringwoodite) ⇔ MgO (periclase) + $MgSiO_3$ (perovskite).

4.4. Implications for δ^{30}Si of the BSE and Si content in the core

Si isotopes could be fractionated during magma ocean cooling process during the early history of the Earth. The prevailing view suggests that the upper and lower mantle formed from crystallization of a hot magma ocean (e.g., Agee, 1993; Walter et al., 2004; Rustad and Yin, 2009; Andrault et al., 2011). From 125 GPa to 2 GPa, the average CN of Si in the melt decreases from six to four with decreasing pressure, lower than the Si CN in perovskite (Stixrude and Karki, 2005; Sanloup et al., 2013). Cooling of the magma ocean led to crystallization of Mg-perovskite,

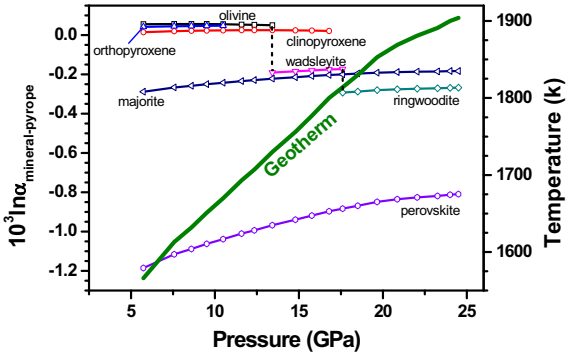

Fig. 4. Si isotope fractionations between garnet (pyrope) and other mantle minerals along the current geotherm gradient. Pyrope is used as a reference because it can coexist with other minerals at the most P–T range of the upper mantle. Olivine has different Si isotope fractionation factors with and wadsleyite and ringwoodite, implying that phase transition can modify Si isotope compositions of mantle minerals. Geotherm data are from Boehler (2000). Isotope fractionation factors are from Table 5.

minor Ca-pervoskite, and periclase from the bottom (Walter and Trønnes, 2004), which formed the lower mantle until the temperature at the lower–upper mantle boundary reached the solidus of peridotite (Fig. 5a) (~2300 °C at 670 km (Walter et al., 2004; Walter and Trønnes, 2004)). Consequently, Si isotopes could be fractionated between the crystallized minerals and the residual melt during magma ocean solidification.

Since the pressure and temperature ranges required for the coexistence of melt and crystals in the mantle are narrow (Walter and Trønnes, 2004), a simple fractional crystallization process is applied to estimate Si isotope fractionation between minerals and melt during the formation of the lower mantle from a crystallizing magma ocean. Mg-perovskite is the dominant Si-bearing minerals in the lower mantle. The effect of the Ca-perovskite on the Si isotopic composition of the lower mantle is negligible because (1) Ca-perovskite is a minor mineral (5% in volume) compared to the Mg-perovskite (Kaminsky, 2012), and (2) the Si isotopic fractionation between Ca-perovskite and Mg-perovskite is most likely very small since Si has the same CN in both minerals. The melt contains Si with CN ranging from 4 to 7. Following Stixrude and Karki (2005) that the average Si CN of melt increases linearly with pressure, the bulk isotope fractionation between crystallizing mineral assemblage and residual melt (bulk $10^3 \ln \alpha_{pv\text{-}melt}$) can be calculated by the following equation:

$$\Delta^{30}Si_{pv\text{-}melt} = f_{IV_{Si}}\Delta^{30}Si_{pv\text{-}IV_{Si_{melt}}} + f_{V_{Si}}\Delta^{30}Si_{pv\text{-}V_{Si_{melt}}} + f_{VI_{Si}}\Delta^{30}Si_{pv\text{-}VI_{Si_{melt}}} + f_{VII_{Si}}\Delta^{30}Si_{pv\text{-}VII_{Si_{melt}}} \quad (4)$$

where $f_{IV_{Si}}$, $f_{V_{Si}}$, $f_{VI_{Si}}$, and $f_{VII_{Si}}$ are the fractions of Si in the melt with CN of 4, 5, 6, and 7, respectively; $\Delta^{30}Si_{pv\text{-}IV_{Si_{melt}}}$ is the fractionation factor between perovskite and fourfold coordinated Si in the melt (similar expressions for the five, six, and sevenfold coordinated Si). Fractions of Si in melt with different CNs at variable pressures can be obtained from Stixrude and Karki (2005). Si isotopic composition in the melt is assumed to be homogeneous because of intensive convection and mixing. We obtain $\Delta^{30}Si_{upper\ mantle\text{-}BSE} = 0.05–0.08‰$ (Fig. 5b) (Supplementary information), which is comparable to the Si isotopic offset between carbonaceous and ordinary chondrites and the BSE (e.g., Georg et al., 2007; Armytage et al., 2011; Fitoussi and Bourdon, 2012; Savage and Moynier, 2013). Using $\delta^{30}Si_{upper\ mantle} = -0.29 \pm 0.08‰$ (Savage et al., 2010), that the $\delta^{30}Si_{BSE}$ is estimated as −0.34‰ to −0.37‰, and $\Delta^{30}Si_{upper\ mantle-lower\ mantle}$ of 0.08‰ to 0.12‰ (Fig. 4b) (see Supplementary information). This upper and lower mantle difference was generated during the solidification of the magma ocean. If the primordial perovskite-rich lower mantle can be partially preserved or isolated from mantle convection since its formation, the primordial feature of a light $\delta^{30}Si_{lower\ mantle}$ could be partially preserved but with a much smaller extent, i.e., $\Delta^{30}Si_{upper\ mantle-lower\ mantle}$ less than 0.08–0.12‰.

$\delta^{30}Si_{BSE}$ is critical in estimating Si content in the core by mass balance calculation using Si isotope difference between BSE and the chondritic reservoir (e.g., Georg et al., 2007; Fitoussi et al., 2009; Ziegler et al., 2010;

Table 5
The reduced partition function ratios for $^{30}Si/^{28}Si$ ($10^3 \ln \beta_{30-28}$) of mantle minerals along the present geothermal gradient to the top of the lower mantle.

P (GPa)	*T* (K)	Olivine	cpx	opx	wds	rwd	maj	prp	Pv
5.74	1566	3.070	3.029	3.056	2.764	2.600	2.726	3.015	1.830
7.57	1613	2.928	2.891	2.916	2.641	2.486	2.605	2.872	1.756
8.60	1632	2.878	2.844	2.868	2.600	2.449	2.564	2.822	1.734
9.51	1651	2.830	2.798	2.821	2.559	2.412	2.524	2.774	1.711
10.49	1670	2.781	2.750	2.774	2.517	2.373	2.484	2.726	1.688
11.59	1693	2.724	2.695	2.718	2.469	2.329	2.436	2.670	1.660
12.35	1707	2.692	2.664	2.688	2.442	2.305	2.410	2.639	1.646
13.42	1730	2.637	2.611	2.635	2.396	2.262	2.365	2.587	1.619
14.79	1756	2.578	2.554	2.578	2.346	2.217	2.316	2.530	1.590
15.77	1777	2.531	2.509	2.533	2.306	2.180	2.277	2.486	1.567
16.80	1800	2.480	2.460	2.485	2.263	2.141	2.236	2.439	1.542
17.60	1814	2.452	2.433	2.458	2.240	2.120	2.213	2.413	1.530
18.50	1830	2.421	2.402	2.428	2.214	2.097	2.188	2.384	1.515
19.66	1853	2.374	2.357	2.383	2.174	2.060	2.149	2.340	1.492
20.86	1869	2.347	2.331	2.358	2.153	2.042	2.129	2.318	1.482
22.04	1881	2.331	2.315	2.344	2.142	2.033	2.119	2.305	1.479
23.25	1891	2.319	2.305	2.335	2.135	2.028	2.113	2.298	1.479
24.00	1900	2.306	2.292	2.322	2.125	2.019	2.104	2.288	1.475
24.50	1904	2.301	2.288	2.319	2.123	2.018	2.102	2.285	1.476

The geothermal gradient data are from Ref. Boehler (2000). Mineral acronyms: opx, orthopyroxene; cpx, clinopyroxene; ol, olivine; maj, majorite; prp, pyrope; wds, wadsleyite; rwd, ringwoodite; and Pv, Mg-perovskite.

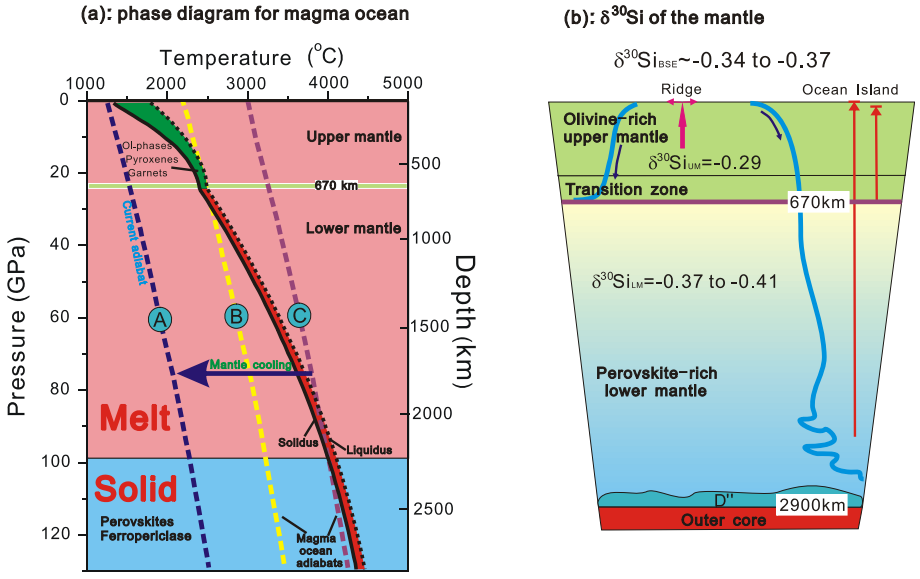

Fig. 5. Si isotope fractionation in the mantle from the magma ocean stage to the present day. (a) At the magma ocean stage, minerals are crystallized from the bottom of the lower mantle due to cooling of the Earth. Si isotopes could be fractionated between the crystallizing mineral (i.e. perovskite) and residual melt. The melt is enriched in heavy Si isotopes. The solidus and liquidus of peridotite are from Walter and Trønnes (2004). Curves A, B, and C represent adiabats over the Earth's history. (b) After the lower mantle formed, the heavier Si isotopic composition is inherited in the upper mantle (UM) above 670 km. The primordial Si isotope fractionation between the upper and lower mantle is preserved from mantle convection until the present day, because the lower mantle is dynamically stable and dense (Karato et al., 1998; Kustowski et al., 2008). $\Delta^{30}Si_{UM\text{-}BSE} = 0.05–0.08‰$ and $\Delta^{30}Si_{UM\text{-}LM} = 0.08–0.12‰$. Taking $\delta^{30}Si_{UM} = -0.29‰$, $\delta^{30}Si_{BSE} = -0.34‰$ to $-0.37‰$ and $\delta^{30}Si_{BSE} = -0.37‰$ to $-0.41‰$ (Supplementary information).

Shahar et al., 2009, 2011). The first order observation on stable isotopes (such as O, Mg, and Si) of the MORBs and mantle peridotites is that they have uniform isotopic compositions, regardless of the differences in the depths of formation, sample locations, ages, mineralogy, and magmatic evolution (e.g., Mattey et al., 1994; Georg et al., 2007; Savage et al., 2010, 2011; Teng et al., 2010; Bourdon et al., 2010; Armytage et al., 2011; Fitoussi and Bourdon, 2012).

This strongly suggests that the upper mantle could be homogenous at a scale larger than mineral grains, either due to effective mixing and diffusion or a lack of preferential separation of isotopically different minerals. Therefore, the MORB and peridotites may be used to represent Si isotopic composition of the upper mantle.

Since the fraction of the isolated primordial lower mantle with light Si isotopic signature is unknown, two extreme scenarios are considered to constrain the Si isotope composition of the BSE. If less than 15% of the primordial lower mantle is isolated from the convecting mantle, then $\delta^{30}Si_{BSE}$ is estimated to be similar to that of the present day upper mantle (Fig. 6). Alternatively, if the primordial lower mantle is completely isolated from the upper mantle, then Si isotope fractionation between the modern upper and lower mantle reflects the primordial features. If this is the case, using $\delta^{30}Si$ of the present day upper mantle as the BSE value would over-estimate the Si content in the core ($[Si]_{core}$) by a few weight percent (Fig. 7). The $[Si]_{core}$ is estimated using a simple mass-balance calculation similar to that was used in Ziegler et al. (2010) and Armytage et al. (2011). Assuming that the core–mantle segregation temperature is ~3000 K (e.g., Wood, 2008), then $\Delta^{30}Si_{silicate\ melt\text{-}metal} = 0.849‰$ (Ziegler et al., 2010). Taking the average $\Delta^{30}Si_{upper\ mantle\text{-}carbonaceous\ chondrite}$ of 0.19‰ (Savage et al., 2013a,b), the $[Si]_{core}$ decreases from 14.1 wt% to 7.3 wt% when $\Delta^{30}Si_{upper\ mantle\text{-}BSE}$ increases from 0 to 0.08‰ (Fig. 7).

4.5. Implications for other stable isotope heterogeneity in the mantle

Si isotope fractionation in the mantle may have an important impact on the applications of other stable isotopic systems in understanding the chemical and isotopic compositions of the Earth. For instance, since Cr^{3+} in almost all important mantle minerals is sixfold coordinated,

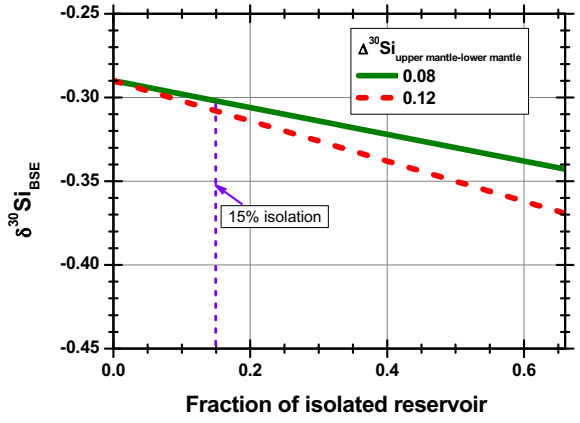

Fig. 6. $\delta^{30}Si_{BSE}$ as a function of the fraction of isolated primordial reservoir in the mantle. Assuming that the fractionation factor of ^{IV}Si in melt is identical to that of ^{IV}Si in olivine or ringwoodite, $\Delta^{30}Si_{upper\ mantle\text{–}lower\ mantle} = 0.12‰$ and 0.08‰, respectively. If the fraction of isolated mantle is zero, $\delta^{30}Si_{BSE} = \delta^{30}Si_{upper\ mantle} = -0.29‰$ (Savage et al., 2010). A completely isolated primordial lower mantle ($f = 0.66$) can decrease $\delta^{30}Si_{BSE}$ from −0.29‰ to −0.34 to 0.37‰.

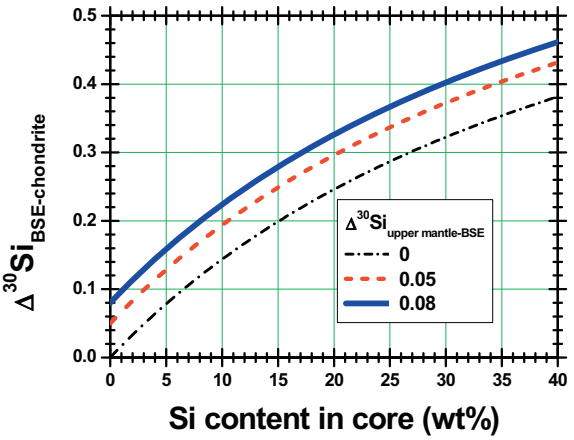

Fig. 7. The effect of Si isotope heterogeneity on estimating the Si content of the core ($[Si]_{core}$). $\Delta^{30}Si_{BSE\text{-}chondrite} = f_{core}[Si]_{core}\Delta^{30}Si_{silicate\text{–}metal}/(f_{BSE}[Si]_{BSE} + f_{core}[Si]_{core})$, where f_{BSE} and f_{core} are the mass fractions of the BSE and the core, respectively; $[Si]_{BSE}$ is the Si content of the BSE. The core-silicate melt equilibrium temperature (T) is fixed to be ~3000 K (Wood, 2008). $\Delta^{30}Si_{BSE\text{-}core} = 7.64 \pm 0.41 \times 10^6/T^2 = 0.849‰$ (Ziegler et al., 2010).

equilibrium fractionation of Cr isotopes between mantle minerals may be negligible relative to current analytical precision. However, for those with significant variations in crystalline environments (e.g., Mg, Ca, Fe, and many others), their isotopes are likely fractionated between mantle minerals at high pressure and temperature conditions (e.g., Huang et al., 2010; Li et al., 2011). These isotopic systems may be heterogeneous at the scales from mineral grains to isolated mantle domains.

5. CONCLUSIONS

Si isotope fractionation factors for mantle silicate minerals (olivine, wadsleyite, ringwoodite, pyroxenes, pyrope, majorite, and Mg-perovskite) are calculated using density functional theory. Our results show that equilibrium fractionation factors of Si isotopes among pyroxenes, olivine, and garnet are negligible relative to current analytical precision (~0.05‰amu^{-1}, 2sd), while Si isotopes can be significantly fractionated among minerals with different Si CNs, e.g., between Mg-perovskite (CN = 6) and olivine polymorphs (CN = 4) and between ^{VI}Si and ^{IV}Si in majorite. Olivine is slightly enriched in heavy Si isotopes compared to wadsleyite, which is enriched in heavy Si isotopes than ringwoodite due to their different crystal structures. Increasing pressure may also slightly reduce Si isotope fractionation factors between silicate minerals. Our calculations further imply that $\Delta^{30}Si_{silicate\text{–}metal}$ obtained by experiments or theoretic calculation at lower pressure may overestimate Si isotope fraction at higher pressure during core formation. Our data also suggest that if the upper and lower mantle formed from crystallizing of a magma ocean, Si isotopes could also be fractionated between the primordial perovskite-rich lower mantle and the primordial upper mantle. If such primordial signature is not completely destroyed and partially preserved through the Earth's history,

significant Si isotope heterogeneity could still exist in the deep mantle. This would have important implications in estimating Si isotope composition of the BSE and Si content in the Earth's core.

ACKNOWLEDGMENTS

This work is financially supported by State Key Development Program of Basic Research of China (2014CB845905), the Natural Science Foundation of China (41173031, 41090370, 41274087), the 111 Project and the Fundamental Research Funds for the Central Universities for F. Huang, the Chinese Academy of Sciences International Partnership Program for Creative Research Teams to Z.Q. Wu, and NSF (EAR-1144727) to S. Huang. Discussion with Liping Qin, Lianxin Wen, Jinshui Huang, Albert Galy, Munir Humayun, and Stein Jacobsen improved the manuscript. We thank Frederic Moynier for comments and editorial handling. We are also grateful to three anonymous reviewers for constructive comments which significantly improve the manuscript. The calculations were conducted in the Shanghai supercomputer centre and the supercomputing centre of the USTC.

APPENDIX A. SUPPLEMENTARY DATA

Supplementary data associated with this article can be found, in the online version, at http://dx.doi.org/10.1016/j.gca.2014.05.035.

REFERENCES

Agee C. B. (1993) Petrology of the mantle transition zone. *Annu. Rev. Earth Planet. Sci.* **21**, 19–41.

Anderson D. L. (1989) *Theory of the Earth*. Blackwell Scientific Publications, Boston.

Andrault D., Bolfan-Casanova N., Nigro G. L., Bouhifd M. A., Garbarino G. and Mezouar M. (2011) Solidus and liquidus profiles of chondritic mantle: implication for melting of the Earth across its history. *Earth Planet. Sci. Lett.* **304**, 251–259.

Angel R. J., Finger L. W., Hazen R. M., Kanzaki M., Weidner D. J., Liebermann R. C. and Veblen D. R. (1989) Structure and twinning of single-crystal Mgsio3 Garnet synthesized at 17 GPa and 1800-degrees-C. *Am. Mineral.* **74**, 509–512.

Armytage R. M. G., Georg R. B., Savage P., Williams H. M. and Halliday A. N. (2011) Silicon isotopes in meteorites and planetary core formation. *Geochim. Cosmochim. Acta* **75**, 3662–3676.

Armytage R. M. G., Georg R. B., Williams H. M. and Halliday A. N. (2012) Silicon isotopes in lunar rocks: implications for the Moon's formation and the early history of the Earth. *Geochim. Cosmochim. Acta* **77**, 504–514.

Baroni S., de Gironcoli S., Dal Corso. A. and Giannozzi P. (2001) Phonons and related crystal properties from density-functional perturbation theory. *Rev. Mod. Phys.* **73**, 515–562.

Bigeleisen J. and Mayer M. G. (1947) Calculation of equilibrium constants for isotopic exchange reactions. *J. Chem. Phys.* **15**, 261–267.

Boehler R. (2000) High-pressure experiments and the phase diagram of lower mantle and core materials. *Rev. Geophys.* **38**, 221–245.

Bourdon B., Tipper T. E., Fitoussi C. and Stracke A. (2010) Chondritic Mg isotope composition of the Earth. *Geochim. Cosmochim. Acta* **74**, 5069–5083.

Cameron M., Sueno S., Prewitt C. T. and Papike J. J. (1973) High-temperature crystal-chemistry of acmite, diopside, hedenbergite, jadeite, spodumene, and ureyite. *Am. Mineral.* **58**, 594–618.

Chakrabarti R. and Jacobsen S. B. (2010) Silicon isotopes in the inner Solar System: implications for core formation, solar nebular processes and partial melting. *Geochim. Cosmochim. Acta* **74**, 6921–6933.

Clayton R. N. (2007) Isotopes: from earth to the solar system. *Annu. Rev. Earth Planet. Sci.* **35**, 1–19.

Dal Corso A., Baroni S., Resta R. and de Gironcoli S. (1993) Ab initio calculation of phonon dispersions in II–VI semiconductors. *Phys. Rev. B* **47**, 3588.

Dewaele A., Fiquet G., Andrault D. and Hausermann D. (2000) P–V–T equation of state of periclase from synchrotron radiation measurements. *J. Geophys. Res.* **105**, 2869–2877.

Fitoussi C. and Bourdon B. (2012) Silicon isotope evidence against an enstatite chondrite Earth. *Science* **335**, 1477–1480.

Fitoussi C., Bourdon B., Kleine T., Oberli F. and Reynolds B. C. (2009) Si isotope systematics of meteorites and terrestrial peridotites: implications for Mg/Si fractionation in the solar nebula and for Si in the Earth's core. *Earth Planet. Sci. Lett.* **287**, 77–85.

Georg R. B., Halliday A. N., Schauble E. A. and Reynolds B. C. (2007) Silicon in the Earth's core. *Nature* **447**, 1102–1106.

Giannozzi P., Baroni S., Bonini N., Calandra M., Car R., Cavazzoni C., Ceresoli D., Chiarotti G. L., Cococcioni M., Dabo I., Dal Corso. A., de Gironcoli S., Fabris S., Fratesi G., Gebauer R., Gerstmann U., Gougoussis C., Kokalj A., Lazzeri M., Martin-Samos L., Marzari N., Mauri F., Mazzarello R., Paolini S., Pasquarello A., Paulatto L., Sbraccia C., Scandolo S., Sclauzero G., Seitsonen A. P., Smogunov A., Umari P. and Wentzcovitch R. M. (2009) QUANTUM ESPRESSO: a modular and open-source software project for quantum simulations of materials. *J. Phys. Condens. Matter* **21**, 395502.

Gibbs G. V. and Smith J. V. (1965) Refinement of crystal structure of synthetic pyrope. *Am. Mineral.* **50**, 2023–2039.

Hazen R., Weinberger M. B., Yang H. and Prewitt C. T. (2000) Comparative high-pressure crystal chemistry of wadsleyite, β-$(Mg_{1-x}Fe_x)_2SiO_4$, with x = 0 and 0.25. *Am. Mineral.* **85**, 770–777.

Hazen R. M. (1976) Effects of temperature and pressure on the crystal structure of forsterite. *Am. Mineral.* **61**, 1280–1293.

Hazen R. M., Downs R. T. and Finger L. W. (1993) Crystal chemistry of ferromagnesian silicate spinels: evidence for Mg–Si disorder. *Am. Mineral.* **78**, 1320–1323.

Hin R. C., Fitoussi C., Schmidt M. W. and Bourdon B. (2014) Experimental determination of the Si isotope fractionation factor between liquid metal and liquid silicate. *Earth Planet. Sci. Lett.* **387**, 55–66.

Horita J., Cole D. R., Polyakov V. B. and Driesner T. (2002) Experimental and theoretical study of pressure effects on hydrogen isotope fractionation in the system brucite-water at elevated temperatures. *Geochim. Cosmochim. Acta* **66**, 3769–3788.

Horiuchi H. and Sawamoto H. (1981) β-Mg_2SiO_4: single-crystal X-ray diffraction study. *Am. Mineral.* **66**, 568–575.

Huang F., Chen L., Wu Z. and Wang W. (2013) First-principles calculations of equilibrium Mg isotope fractionations between garnet, clinopyroxene, orthopyroxene, and olivine: implications for Mg isotope thermometry. *Earth Planet. Sci. Lett.* **367**, 61–70.

Huang S., Farkaš J. and Jacobsen S. B. (2010) Calcium isotopic fractionation between clinopyroxene and orthopyroxene from mantle peridotites. *Earth Planet. Sci. Lett.* **292**, 337–344.

Hushur A., Manghnani M. H., Smyth J. R., Nestola F. and Frost D. J. (2009) Crystal chemistry of hydrous forsterite and its vibrational properties up to 41 GPa. *Am. Mineral.* **94**, 751–760.

Javoy M., Kaminski E., Guyot F., Andrault D., Sanloup C., Moreira M., Labrosse S., Jambon A., Agrinier P., Davaille A. and Jaupart C. (2010) The chemical composition of the Earth: enstatite chondrite models. *Earth Planet. Sci. Lett.* **293**, 259–268.

Kaminski E. and Javoy M. (2013) A two-stage scenario for the formation of the Earth's mantle and core. *Earth Planet. Sci. Lett.* **365**, 97–107.

Kaminsky F. (2012) Mineralogy of the lower mantle: a review of 'super-deep' mineral inclusions in diamond. *Earth Sci. Rev.* **110**, 127–147.

Karato S. I., Dupas-Bruzak C. and Rubie D. C. (1998) Plastic deformation of silicate spinel under the transition-zone conditions of the Earth's mantle. *Nature* **395**, 266–269.

Kempl J., Vroon P. Z., Zinngrebe E. and van Westrenen W. (2013) Si isotope fractionation between Si-poor metal and silicate melt at pressure–temperature conditions relevant to metal segregation in small planetary bodies. *Earth Planet. Sci. Lett.* **368**, 61–68.

Kieffer S. W. (1982) Thermodynamics and lattice-vibrations of minerals. 5. Applications to Phase-equilibria, isotopic fractionation, and high-pressure thermodynamic properties. *Rev. Geophys.* **20**, 827–849.

Kirfel A., Lippmann T., Blaha P., Schwarz K., Cox D. F., Rosso K. M. and Gibbs G. V. (2005) Electron density distribution and bond critical point properties for forsterite, Mg(2)SiO(4), determined with synchrotron single crystal X-ray diffraction data. *Phys. Chem. Miner.* **32**, 301–313.

Kustowski B., Ekström G. and Dziewoński A. M. (2008) Anisotropic shear-wave velocity structure of the Earth's mantle: a global model. *J. Geophys. Res.* **113**, B06306.

Li J. and Agee C. B. (1996) Geochemistry of mantle–core differentiation at high pressure. *Nature* **381**, 686–689.

Li L., Wentzcovitch R. M., Weidner D. J. and Da Silva C. R. S. (2007) Vibrational and thermodynamic properties of forsterite at mantle conditions. *J. Geophys. Res. Solid Earth* **112**, B05206.

Li W.-Y., Teng F.-Z., Xiao Y. and Huang J. (2011) High-temperature inter-mineral magnesium isotope fractionation in eclogite from the Dabie orogen, China. *Earth Planet. Sci. Lett.* **304**, 224–230.

Li X. F., Zhao H., Tang M. and Liu Y. (2009) Theoretical prediction for several important equilibrium Ge isotope fractionation factors and geological implications. *Earth Planet. Sc. Lett.* **287**(1–2), 1–11.

Méheut M., Lazzeri M., Balan E. and Mauri F. (2007) Equilibrium isotopic fractionation in the kaolinite, quartz, water system: prediction from first-principles density-functional theory. *Geochim. Cosmochim. Acta* **71**, 3170–3181.

Méheut M., Lazzeri M., Balan E. and Mauri F. (2009) Structural control over equilibrium silicon and oxygen isotopic fractionation: a first-principles density-functional theory study. *Chem. Geol.* **258**, 28–37.

Méheut M. and Schauble E. A. (2014) Silicon isotope fractionation in silicate minerals: insights from first-principles models of phyllosilicates, albite and pyrope. *Geochim. Cosmochim. Acta* **134**, 137–154.

Mao H. K., Hemley R. J., Fei Y., Shu J. F., Chen L. C., Jephcoat A. P., Wu Y. and Bassett W. A. (1991) Effect of pressure, temperature, and composition on lattice-parameters and density of (Fe, Mg)Sio_3-perovskites to 30 GPa. *J. Geophys. Res.* **96**, 8069–8079.

Mattey D., Lowry D. and Macpherson C. (1994) Oxygen isotope composition of mantle peridotite. *J. Petrol.* **38**, 1331–1358.

McDonough W. F. (2003) Compositional model for the Earth's core. *Treat. Geochem.* **2**, 547–568.

McDonough W. F. and Sun S.-S. (1995) The composition of the Earth. *Chem. Geol.* **120**, 223–253.

Meng Y., Fei Y., Weidner D. J., Gwanmesia G. D. and Hu J. (1994) Hydrostatic compression of gamma-Mg_2SiO_4 to mantle pressures and 700-K – thermal equation of state and related thermoelastic properties. *Phys. Chem. Miner.* **21**, 407–412.

Moynier F., Yin Q.-Z. and Schauble E. (2011) Isotopic evidence of Cr partitioning into earth's core. *Science* **331**, 1414–1420.

Perdew J. P. and Zunger A. (1981) Self-interaction correction to density-functional approximations for many-electron systems. *Phys. Rev. B* **23**, 5048–5079.

Polyakov V. B. (2009) Equilibrium iron isotope fractionation at core–mantle boundary conditions. *Science* **323**, 912–914.

Pringle E. A., Savage P., Badro J., Barrat J. and Moynier F. (2013) Redox state during core formation on asteroid 4-Vesta. *Earth Planet. Sci. Lett.* **373**, 75–82.

Rustad J. R. and Yin Q.-Z. (2009) Iron isotope fractionation in the Earth's lower mantle. *Nat. Geosci.* **2**, 514–518.

Sanloup C., Drewitt W. E. J., Konopkova Z., Dalladay-Simpson P., Morton D. M., Rai N., van Westrenen W. and Morgenroth W. (2013) Structural change in molten basalt at deep mantle conditions. *Nature* **503**, 104–107.

Savage P., Georg R. B., Armytage R. M. G., Williams H. M. and Halliday A. N. (2010) Silicon isotope homogeneity in the mantle. *Earth Planet. Sci. Lett.* **295**, 139–146.

Savage P., Georg R. B., Williams H. M., Burton K. W. and Halliday A. N. (2011) Silicon isotope fractionation during magmatic differentiation. *Geochim. Cosmochim. Acta* **75**, 6124–6139.

Savage P., Georg R. B., Williams H. M. and Halliday A. N. (2013a) The silicon isotope composition of the upper continental crust. *Geochim. Cosmochim. Acta* **109**, 384–399.

Savage P., Georg R. B., Williams H. M., Turner S., Halliday A. N. and Chappell B. W. (2012) The silicon isotope composition of granites. *Geochim. Cosmochim. Acta* **92**, 184–202.

Savage P., Wimpenny J., Harvey J., Yin Qing-Zhu and Moynier F. (2013b) Investigating the effects of abyssal peridotite alteration on Si, Mg and Zn isotopes, AGU Fall meeting, V54A-06 abstract.

Savage P. S. and Moynier F. (2013) Silicon isotopic variation in enstatite meteorites: clues to their origin and Earth-forming material. *Earth Planet. Sci. Lett.* **361**, 487–496.

Savage P., Armytage R., Bastian Georg R. and Halliday A. N. (2014) High temperature silicon isotope geochemistry. *Lithos* **190–191**, 500–519.

Schauble E. A. (2011) First-principles estimates of equilibrium magnesium isotope fractionation in silicate, oxide, carbonate and hexaaquamagnesium(2+) crystals. *Geochim. Cosmochim. Acta* **75**, 844–869.

Shahar A., Hillgren V. J., Young E. D., Fei Y., Macris C. A. and Deng L. (2011) High-temperature Si isotope fractionation between iron metal and silicate. *Geochim. Cosmochim. Acta* **75**, 7688–7697.

Shahar A., Ziegler K., Young E. D., Ricolleau A., Schauble E. A. and Fei Y. (2009) Experimentally determined Si isotope fractionation between silicate and Fe metal and implications for Earth's core formation. *Earth Planet. Sci. Lett.* **288**, 228–234.

Stixrude L. and Karki B. (2005) Structure and freezing of $MgSiO_3$ liquid in Earth's lower mantle. *Science* **320**, 297–299.

Teng F.-Z., Li W.-Y., Ke S., Marty B., Dauphas N., Huang S., Wu F.-Y. and Pourmand A. (2010) Magnesium isotopic composition of the Earth and chondrites. *Geochim. Cosmochim. Acta* **74**, 4150–4166.

Troullier N. and Martins J. L. (1991) Efficient pseudopotentials for plane-wave calculations. 2. Operators for fast iterative diagonalization. *Phys. Rev. B* **43**, 8861–8869.

Tsuchiya T., Tsuchiya J., Umemoto K. and Wentzcovitch R. A. (2004) Phase transition in $MgSiO_3$ perovskite in the earth's lower mantle. *Earth Planet. Sci. Lett.* **224**, 241–248.

Urey H. C. (1947) The thermodynamic properties of isotopic substances. *J. Chem. Soc. (Lond.)*, 562–581.

Vanderbilt D. (1990) Soft self-consistent pseudopotentials in a generalized eigenvalue formalism. *Phys. Rev. B* **41**, 7892–7895.

Wade J. and Wood B. J. (2005) Core formation and the oxidation state of the Earth. *Earth Planet. Sci. Lett.* **236**, 78–95.

Walter M. J., Nakamura E., Trønnes R. G. and Frost D. J. (2004) Experimental constraints on crystallization differentiation in a deep magma ocean. *Geochim. Cosmochim. Acta* **68**, 4267–4284.

Walter M. J. and Trønnes R. G. (2004) Early Earth differentiation. *Earth Planet. Sci. Lett.* **225**, 253–269.

Wentzcovitch R. M. (1991) Invariant molecular-dynamics approach to structural phase-transitions. *Phys. Rev. B* **44**, 2358–2361.

Wentzcovitch R. M., Yu Y. G. and Wu Z. (2010) Thermodynamic properties and phase relations in mantle minerals investigated by first principles quasiharmonic theory. *Rev. Mineral. Geochem.* **71**, 59–98.

Wood B. J. (2008) Accretion and core formation: constraints from metal–silicate partitioning. *Phil. Trans. R. Soc. Lond.* **366**, 4339–4355.

Wu Z. and Wentzcovitch R. M. (2007) Vibrational and thermodynamic properties of wadsleyite: a density functional study. *J. Geophys. Res.* **112**, B12202.

Wu Z., Wentzcovitch R. M., Umemoto K., Li B. S., Hirose K. and Zheng J. C. (2008) Pressure–volume–temperature relations in MgO: an ultrahigh pressure–temperature scale for planetary sciences applications. *J. Geophys. Res.* **113**, B06204.

Yang H. X. and Ghose S. (1995) High-temperature single-crystal X-ray-diffraction studies of the ortho-proto phase-transition in enstatite, $Mg_2Si_2O_6$ at 1360 K. *Phys. Chem. Miner.* **22**, 300–310.

Yu Y. G. G. and Wentzcovitch R. M. (2006) Density functional study of vibrational and thermodynamic properties of ring-woodite. *J. Geophys. Res.* **111**, B12202.

Yu Y. G. G., Wentzcovitch R. M. and Angel R. J. (2010) First principles study of thermodynamics and phase transition in low-pressure (P2(1)/c) and high-pressure (C2/c) clinoenstatite $MgSiO_3$. *J. Geophys. Res.* **115**, B02201.

Yu Y. G. G., Wentzcovitch R. M., Vinograd V. L. and Angel R. J. (2011) Thermodynamic properties of $MgSiO_3$ majorite and phase transitions near 660 km depth in $MgSiO_3$ and Mg_2SiO_4: a first principles study. *J. Geophys. Res.* **116**, B02208.

Yu Y. G. G., Wu Z. and Wentzcovitch R. M. (2008) Alpha–beta–gamma transformations in Mg_2SiO_4 in Earth's transition zone. *Earth Planet. Sci. Lett.* **273**, 115–122.

Zambardi T. and Poitrasson F. (2011) Precise determination of silicon isotopes in silicate rock reference materials by MC-ICP-MS. *Geost. Geoanal. Res.* **35**, 89–99.

Zambardi T., Poitrasson F., Corgne A., Méheut M., Quitté G. and Anand M. (2013) Silicon isotope variations in the inner solar system: implications for planetary formation, differentiation and composition. *Geochim. Cosmochim. Acta* **121**, 67–83.

Ziegler K., Young E. D., Schauble E. A. and Wasson J. T. (2010) Metal–silicate silicon isotope fractionation in enstatite meteorites and constraints on Earth's core formation. *Earth Planet. Sci. Lett.* **295**, 487–496.

Associate editor: Frederic Moynier